



**Topology-mediated electro-optical behaviour of wide-temperature liquid crystalline amorphous blue phase**

Journal:	<i>Soft Matter</i>
Manuscript ID:	SM-ART-07-2015-001918.R1
Article Type:	Paper
Date Submitted by the Author:	15-Aug-2015
Complete List of Authors:	Kim, Min Su; Kent State University, Chemical Physics and Liquid Crystal Institute Chien, Liang-Chy; Kent State University, Chemical Physics and Liquid Crystal Institute



Journal Name

ARTICLE

## Topology-mediated electro-optical behaviour of wide-temperature liquid crystalline amorphous blue phase†

Min Su Kim\*<sup>a</sup> and Liang-Chy Chien<sup>a</sup>Received 00th January 20xx,  
Accepted 00th January 20xx

DOI: 10.1039/x0xx00000x

www.rsc.org/

Wide-temperature liquid crystalline amorphous blue phase based on polymer network stabilization exhibits high thermodynamic stability with the extended temperature range from a few °C to more than 80 °C including room temperature. Analyses using confocal laser scanning microscopy show that the polymer network imitates the aperiodic disclination-entangled structure of amorphous blue phase and entails highly intertwined interaction with liquid crystal molecules. The stabilized amorphous blue phase manifests tens of microsecond response time, a consistent achromatic dark state and intrinsically hysteresis-free during application of an electric field. The topological and electro-optical features of the stabilized amorphous blue phase are further compared with the stabilized isotropic and cubic blue phases. These results not only provide a physical perspective in electro-optical response of a liquid crystal and polymer composite but also open up new direction to electro-optical device applications.

### Introduction

Liquid crystalline blue phases (BPs, known as BPI with face-centered cubic, BPII with body-centered cubic, and BPIII with amorphous structure) are of interest in their physical and optical perspectives such as theories regarding liquid crystal physics,<sup>1–5</sup> numerical modelling,<sup>6–10</sup> unique electro-optical behaviour,<sup>11–16</sup> various stability control techniques,<sup>17–24</sup> display and photonic device applications.<sup>25–30</sup> Lately, the structure of amorphous BP (BPIII) has been well modelled<sup>31</sup> and confirmed by experimental visualization of disclinations with polymer molding.<sup>32</sup> The structural difference in cubic BPs and BPIII inspires and encourages further research on liquid crystal physics and applications. Despite of the fast switching time of BPs, their high driving voltage, selective Bragg reflection, and electro-optical hysteresis are crucial for device applications. The approaches to overcome those obstacles have been reported; for example, 1) high driving voltage is possibly reduced using protruded electrodes,<sup>33</sup> high dielectric anisotropy of liquid crystals and high Kerr constant materials.<sup>34,35</sup> 2) Bragg reflection, which is related to the chiral pitch of liquid crystals, becomes invisible by controlling the chiral pitch out of visible range.<sup>36</sup> However, to the best of our knowledge, achieving chirality for infrared range of lattice size to appear cubic BPs has not been reported. To achieving the ultraviolet range, it requires short chiral pitch with less than around 150 nm and also contributes to a high driving voltage.

On the other hand, polymer-stabilized isotropic phase and spontaneous formation of optically isotropic nematic phase have been proposed because of its perfect dark state property, but it exhibits the electro-optical hysteresis.<sup>37–39</sup> 3) Suppression of the electro-optical hysteresis has been reported by controlling polarization of illumination, photopolymerization density near electrodes, or constituting nanoparticle additives in a cubic BP cell.<sup>40–43</sup> The reason of the hysteresis has also been explained by an electrostriction effect and/or a non-uniformity of lattice orientation up on each grain of cubic BPs.<sup>11,16,44</sup> Nonetheless, suppressing or controlling such intrinsic electro-optical behaviour of cubic BPs requires overcoming big challenges in thermodynamic perspectives. The BPIII has meanwhile been researched as an another candidate, but limitations remain with both extension of existing temperature range and detailed identification of electro-optical response.<sup>45–47</sup>

Here, we demonstrate wide-temperature range BPIII (> 80 °C) achieved by polymer-stabilization, where the composite shows no Bragg reflection, no grain boundary, and no hysteresis in the electro-optical response. We further elucidate the topological behaviours under the electric switching of the stabilized BPIII, isotropic phase and BPI by confocal laser scanning microscopy (CLSM). The topology-mediated electro-optical behaviour in the stabilized phases provides insights into key issues such as the interfacial interactions and the electro-optical responses in the stabilized phases.

### Experimental

#### Materials and methods

<sup>a</sup> Liquid Crystal Institute & Chemical Physics Interdisciplinary Program, Kent State University, Kent, OH 44242, USA. \*E-mail: [mkim12@kent.edu](mailto:mkim12@kent.edu)

†Electronic Supplementary Information (ESI) available: Videos S1–S3. See DOI: 10.1039/x0xx00000x

**Polymer and liquid crystal composite.** Liquid crystals (HCCH, HTG135200-100,  $\Delta n = 0.204 @ 589 \text{ nm}$ ,  $20 \text{ }^\circ\text{C}$ ,  $\Delta\varepsilon = +57.2 @ 1 \text{ kHz}$ ,  $25 \text{ }^\circ\text{C}$ ) were mixed with a chiral dopant (HCCH, R5011, Helical twisting power  $\sim 110 \mu\text{m}^{-1} @ 25 \text{ }^\circ\text{C}$ ) and reactive monomer composite consisting of a mesogenic diacrylate monomer (Merck, RM257) and difunctional acrylate monomer (Aldrich, Bisphenol A dimethacrylate). Prior to the curing, the polymer and liquid crystal composite was characterized by mapping the phase diagram with respect to temperature, chiral fraction and chirality. In order to accelerate photo-polymerization, a small amount of photo-initiator (Aldrich, Irgacure 651) was added to the polymer and liquid crystal composite. (See Table 1)

**Table 1** The concentration of polymer and liquid crystal composites, and photo-polymerization temperature (See Fig. 1 for samples before and after photo-polymerization).

Sample phase	LC <sup>c</sup>	Concentration [wt%] <sup>a</sup>				T <sub>ph</sub> <sup>b</sup> [°C]
		CD <sup>d</sup>	M1 <sup>e</sup>	M2 <sup>f</sup>	PI <sup>g</sup>	
BPIII	73.6	4.4 <sup>g</sup>	19.9	2.1	0.1	83.0
Iso <sup>h</sup>	73.6	4.4 <sup>g</sup>	19.9	2.1	0.1	87.0
BPI	74.0	3.8 <sup>g</sup>	20.0	2.1	0.1	82.5

<sup>a</sup> Element weight to composite weight. <sup>b</sup> Photo-polymerization temperature. Denotations: <sup>c</sup> liquid crystal (HTG135200-100), <sup>d</sup> chiral dopant (R5011) <sup>e</sup> monomer1 (RM257), <sup>f</sup> monomer2 (Bisphenol A dimethacrylate), and <sup>g</sup> Photo-initiator (Irgacure651). <sup>h</sup> Isotropic phase.

**Cell fabrication.** A glass substrate was deposited by indium-tin-oxide and patterned to have interdigitated electrodes to apply an in-plane electric field, and then assembled to a plane glass substrate using ultraviolet curable adhesive (Noland, NOA65), which was mixed with  $10 \mu\text{m}$  spherical spacers for a uniform cell gap. The cell, capillary-injected by polymer and liquid crystal composite, was loaded on to a hot stage with a calibrated temperature controller (Instec, Inc., precision of  $\pm 0.1 \text{ }^\circ\text{C}$ ). The reactive monomers in the composite were photo-polymerized at designated temperatures using collimated ultraviolet (Uvata, spot UV LED) with irradiance of  $0.8 \text{ mW cm}^{-2}$  at  $365 \text{ nm}$  while the phases were monitored by a polarizing optical microscope (Nikon, Corp.). (See Table 1.) The photographs of cells were taken by a digital camera.

### Characterization

**Phase diagram and Reflection spectra.** Photomicrographs were automatically acquired while temperature was ramped up and down for verification of the phase sequence. Cubic BPs were examined by the textures. The BPIII was distinguished from isotropic phase by observing optical activity in BPIII. The optical activity in BPIII was confirmed by photomicrographs taken at a few degrees of positive and negative deviation angles between an analyzer and a polarizer. The reflection spectra were measured by a spectrometer (Ocean Optics, USB2000+) from a collimated Tungsten-halogen light source (Ocean Optics, LS-1) after photo-polymerization.

**Electro-optic measurement.** Cells with the stabilized phases were placed between crossed polarizers and maintained the directions of electric fields at  $45^\circ$  to the optic axes of crossed polarizers. A photodiode detector was used to detect the transmitted light from laser light sources (He-Ne:  $\lambda = 633 \text{ nm}$ , Ar-ion:  $514, 460 \text{ nm}$ ), while an electric field was applied to the interdigitated electrode in the cells. Both input and output signals were controlled by homemade software via a terminal block (National Instruments, Corp., BNC-2090).

**Confocal laser scanning microscopy (CLSM).** In order to acquire the images with high magnification, a short wavelength laser light ( $\lambda = 408 \text{ nm}$ ) was equipped in a confocal laser scanning microscope (Olympus, LEXT OLS3100) with minimized optical aberrations. For preparation of the samples, a thin top glass substrate ( $< 100 \mu\text{m}$ ) was assembled onto the substrate with the interdigitated electrodes to satisfy the working distance of an objective lens with high magnification.

## Results and discussions

Photomicrographs before photo-polymerization are taken at BPIII ( $83 \text{ }^\circ\text{C}$ ), isotropic phase ( $87 \text{ }^\circ\text{C}$ ), and BPI ( $82.5 \text{ }^\circ\text{C}$ ) as shown in Fig. 1a. At deviation angles between an analyzer and a polarizer  $\beta = \pm 3^\circ$ , the color of images become bluish and yellowish for negative and positive  $\beta$  owing to the optical activity in BPIII, which is distinguished from isotropic phase. The color difference at the deviation angles in BPIII (Video S1) is caused due to optical activity.<sup>48</sup> The optic axis of plane-polarized light after the polarizer become rotated when traveling BPIII layer, so that the optic axis of polarization deviates from the optic axis of the analyzer. The deviation at positive and negative angles contributes differently to corresponding wavelength ranges.

The target phases for polymer-stabilization are indicated with red, black and green stars for BPIII, isotropic phase and BPI, respectively, in the phase diagram (Fig. 1b). Phase transitions from BPIII to isotropic phase at  $\beta = 5^\circ$  (with chiral fraction  $\sim 4.72 \%$ ) and from BPIII to BPI (with chiral fraction  $\sim 3.98 \%$ ) are shown in Video S1 and S2, respectively. After polymer-stabilization (see materials and methods), the stabilized phases are well maintained over  $80 \text{ }^\circ\text{C}$  (the range of the stabilized BPIII is below  $0 \text{ }^\circ\text{C}$  to  $87 \text{ }^\circ\text{C}$ ) as shown in Fig. 1c, d. The photos of the cells and the photomicrographs show similar dark states for BPIII and isotropic phase, whereas BPI shows light leakage corresponding to Bragg diffraction. Moreover, the reflectance measurements are in good agreement with the photomicrographs observed by reflection mode as shown in Fig. 2. We note that the reflection spectra of the stabilized BPIII and isotropic phase reveal similar behaviours, only slightly higher reflectance of the stabilized BPIII than that of the isotropic phase near short-wavelength range, whereas a peak or seemingly overlapped multiple peaks are measured in the stabilized BPI.

Electro-optical switching behaviour of the stabilized BPIII can be explained by Kerr effect<sup>49</sup> described as  $\Delta n_{\text{ind}}(E) = \lambda KE^2$ , in which  $\Delta n_{\text{ind}}$  is the birefringence induced by an applied electric

field  $E$ , under a constraint,  $\Delta n_{\text{ind}}(E) \leq \Delta n_{\text{sat}}(E_s)$  with saturated birefringence  $\Delta n_{\text{sat}}$  of host liquid crystals induced by the saturation electric field  $E_s$ ,  $\lambda$  is the wavelength of light, and  $K$  is the Kerr constant. When the direction of the applied electric field is  $45^\circ$  to the crossed polarizers, the detected light intensity  $I$  can be given as

$$I = I_0 \sin^2 \left( \frac{\pi d \Delta n_{\text{ind}}}{\lambda} \right) \quad (1)$$

where  $d$  denotes cell gap that light is traveling inside a cell. The switching of the stabilized BPIII cell from the dark state to bright state and back to dark state is shown in Fig. 3a and b. The corresponding photomicrographs of the switching behaviour (Fig. 3b and Video S3) exhibit excellent optical contrast between the field-off and field-on states. The on-state photomicrograph shows a large field-induced birefringence in between the electrodes and the stripes indicate that no electric field contributes to the induced birefringence on the center of the electrodes. The electro-optical behaviours of the stabilized cells are investigated with transmittance versus applied electric fields curves with red, green, and blue (RGB) light sources for BPIII (Fig. 3c), isotropic phase (Fig. 3d) and BPI (Fig. 3e).<sup>‡</sup> (See Materials and methods). The hysteresis is defined as  $H = (E_{\text{asc}} - E_{\text{des}}) / E_p \times 100 \%$ , where  $E_p$  denotes electric fields at peak intensity, and  $E_{\text{asc}}$  and  $E_{\text{des}}$  denote half of the peak during ascending and descending electric fields, respectively. The measured hysteresis  $H$  with RGB light sources is minimum for the stabilized BPIII (Fig. 3c; R: 0.5 %, G: 0.5 %, B: 2.2 %), but is significant for the stabilized isotropic phase (Fig. 3d; R: 6.0 %, G: 8.8 %, B: 11.3 %) and relatively less significant for the stabilized BPI (Fig. 3e; R: 5.9 %, G: 3.7 %, B: 4.2 %).

The photomicrographs of the stabilized isotropic phase and BPI cells are taken before, after and several tens of minutes after applying an electric field. The residual light leakage near the edge of the electrodes in both cells is shown in Fig. 4, whereas the stabilized BPIII shows consistent dark state before and after applying an electric field as shown in Fig. 3a and b. After several tens of minutes, the residual light leakage still remains for the stabilized isotropic phase but disappears in BPI. We may deduce that the electrostriction effect in the stabilized BPI responds for several minutes, and the switching mechanism of the stabilized isotropic phase is apparently distinguished from the stabilized BPIII.

To identify the differences in the electro-optical switching in detail, direct observation and thorough investigation of topology at a focal plane near the electrodes in stabilized cells are done by CLSM (Fig. 5). The CLSM images manifest stronger reflection on the electrodes. The stabilized BPIII reveals consistent isotropy in topology before and after the applied electric field (Fig. 5a, c and insets) while it shows spatially different structural deformation between electrodes under the applied electric field,  $E = 18.5 \text{ V}/\mu\text{m}$  (Fig. 5b and inset). The deformation is more severe upon the edge of the electrode due to the relatively stronger electric field strength. Comparing the topology of the stabilized BPIII and isotropic phase, the

reflected intensity in short-range is quite non-uniform in BPIII, unlike in isotropic phase. In BPIII, reactive monomers are more miscible in disclinations of BPIII. Consequently, polymerization occurs around disclinations; the polymer network actually imitates the disclinations in BPIII (Schematic illustrations in Fig. 5a-c).<sup>32</sup> In isotropic phase, on the contrary, the short-range reflection is relatively uniform (Fig. 5d-f and insets) although the overall topology is similar to that of the stabilized BPIII. During photo-polymerization, phase separation occurs in isotropic phase. The entropy-driven randomness guides the polymer network growing bulky, and liquid crystals are confined in a pore-type space such as the polymer-dispersed liquid crystal (Schematic illustrations in Fig. 5d-f).<sup>50</sup> In the center region of the pore, liquid crystal molecules are not anchored strongly enough to memorize their original orientations due to relatively low anchoring strength (Schematic illustration in Fig. 5f and Fig. 4a). The analysis strongly supports the reason that residual light leakage is generated in the isotropic phase. In the stabilized BPI, on the other hand, the topology reveals grains with boundaries, and each grain consists of the periodic lattice structure (Fig. 5g-i). The periodic lattices are deformed under the applied electric field, i.e., electrostriction effect takes place (Insets of Fig. 5h). After applying the electric field, the topological deformation in the periodic undulations remains (Fig. 5i) as well as shown in the polarizing optical micrograph in Fig. 4b.

Figure 6 shows the electro-optical response times of the stabilized cells. Both rise and decay times are measured between 10 % and 90 % transmittance changes. In the stabilized BPIII, the response time is less than 100  $\mu\text{s}$  for both rise and decay (Fig. 6a, b). In case of the stabilized isotropic phase, the low anchoring strength gives rise to slow decay time with respect to the interaction between liquid crystal molecules and polymer network (Fig. 6a, c). Although the response time of BPI is still in sub-millisecond range, decay time is much slower than that of the stabilized BPIII at every RGB light sources (Fig. 6a, d).

**Table 2** The properties of the stabilized phases.

Stabilized phase	$E_s^a$ [V/ $\mu\text{m}$ ]	$H^b$ [%]	$\tau_d^c$ [ms]	Stability [ $^\circ\text{C}$ ]	Topology
BPIII	~ 18.5	0.49	0.07	> 83.0	Isotropic <sup>d</sup>
Iso <sup>f</sup>	~ 11.0	8.78	5.70	> 87.0	Isotropic <sup>d</sup>
BPI	~ 17.0	3.74	0.61	> 82.5	Grains and boundaries with periodic undulations

<sup>a</sup> The saturation electric field. <sup>b</sup> Hysteresis at wavelength of 514 nm. <sup>c</sup> RGB average decay time. <sup>d</sup> Although the topology is isotropic for both phases, the short-range order of the stabilized BPIII differs from that of the stabilized isotropic phase. <sup>f</sup> Abbreviated from isotropic phase.

Here we discuss more aspects of the results. Under the polarizing optical microscope, isotropic phase shows no color due to the symmetry. Cubic BPs also imply an optically isotropic state owing to the cubic symmetry, but colorful

platelet and/or mosaic type textures are observed because of Bragg reflection. The symmetry of BPIII is similar to that of isotropic phase and has neither long-range order nor structural periodicity. However, previous study on scattering property of the BPIII differs from that of isotropic phase due to dissimilarity in short-range orders<sup>51</sup> as also shown in the measured reflectance (Fig. 2) In the CLSM images of the stabilized BPIII and isotropic phase observed at the focal plane (Insets of Fig. 5a, d), the different localized reflection may refer to the surface roughness and also may imply the structural and topological difference between the stabilized BPIII and isotropic phase.

The degree of hysteresis upon the applied electric fields in the stabilized BPIII and isotropic phase tends to be high at short wavelength, which is consistent with the Kerr effect as defined in Eq. (1). However, the opposite tendency is found for the stabilized BPI (Fig. 3 and Table 2). The reason is deduced that the electrostriction effect and/or complex topology contribute to the electric switching as well. As the lattice is elongated along the electric field, which is perpendicular to the direction of light traveling, the wavelength range corresponding to transmittance shifts to long wavelength range.

The main features of the stabilized phases are shown in Table 2. The saturation electric field of the stabilized BPIII is approximately 1.68 and 1.09 times higher than that of the stabilized isotropic phase and BPI, respectively. However, the stabilized BPIII achieves excellent achromatic dark state, 17.9 and 7.6 times less hysteresis at wavelength of 514 nm, and 81.4 and 8.7 times faster response time than that of the stabilized isotropic phase and BPI, respectively.

## Conclusions

Wide-temperature liquid crystalline amorphous blue phase has been demonstrated by polymer network stabilization. The stabilized amorphous blue phase shows tens of microsecond switching time, hysteresis-free and a consistent achromatic dark state during application of an electric field. The topology-mediated electro-optical behaviour verifies that such strong anchoring strength in the stabilized amorphous blue phase is allowed by polymer network that imitates the three-dimensionally tangled disclinations. We believe that these results will meaningfully contribute to the physical interest in amorphous blue phase and to the design of future electro-optical device applications.

## Notes and references

§ The concentration of the chiral dopant deviates from the chiral fraction in phase diagram (Fig. 1b) because the definition of chiral fraction in Fig. 1b is weight of the chiral dopant to the weight of the mesogenic constituents, which are liquid crystals (HTG135200-100) and reactive mesogen (RM257).

‡ The measured transmittance was normalized by the lowest and highest intensities of each measurement, and the cells had been driven for several times before the measurements of transmittance versus an applied electric field. Consequently, the transmittance at

the minimum electric fields in ascending and descending fields implies similar brightness level, i.e., the field-off states before and after driving had already experienced the electric field in Fig. 3.

- 1 D. C. Wright and N. D. Mermin, *Rev. Mod. Phys.*, 1989, **61**, 385–432.
- 2 S. Meiboom, J. P. Sethna, P. W. Anderson and W. F. Brinkman, *Phys. Rev. Lett.*, 1981, **46**, 1216–1219.
- 3 H. Grebel, R. M. Hornreich and S. Shtrikman, *Phys. Rev. A*, 1984, **30**, 3264–3278.
- 4 P. P. Crooker, *Chirality in Liquid Crystals*, Springer-Verlag, New York, 2001.
- 5 P.-G. de Gennes and J. Prost, *The Physics of Liquid Crystals*, Clarendon Press, 1993.
- 6 G. P. Alexander and J. M. Yeomans, *Phys. Rev. E*, 2006, **74**, 061706.
- 7 J. Fukuda and S. Zumer, *Nat. Commun.*, 2011, **2**, 246.
- 8 O. Henrich, K. Stratford, M. E. Cates and D. Marenduzzo, *Phys. Rev. Lett.*, 2011, **106**, 107801.
- 9 O. Henrich, K. Stratford, D. Marenduzzo and M. E. Cates, *Proc. Natl. Acad. Sci. U. S. A.*, 2010, **107**, 13212–5.
- 10 M. Ravnik, G. P. Alexander, J. M. Yeomans and S. Žumer, *Proc. Natl. Acad. Sci. U. S. A.*, 2011, **108**, 5188–92.
- 11 H. Choi, H. Higuchi and H. Kikuchi, *Soft Matter*, 2011, **7**, 4252.
- 12 A. Tiribocchi, G. Gonnella, D. Marenduzzo and E. Orlandini, *Soft Matter*, 2011, **7**, 3295.
- 13 F. Porsch and H. Stegemeyer, *Chem. Phys. Lett.*, 1989, **155**, 620–623.
- 14 H. Stark and H.-R. Trebin, *Phys. Rev. A*, 1991, **44**, 2752–2755.
- 15 H. Stegemeyer and F. Porsch, *Phys. Rev. A*, 1984, **30**, 3369–3371.
- 16 D. Xu, J. Yan, J. Yuan, F. Peng, Y. Chen and S.-T. Wu, *Appl. Phys. Lett.*, 2014, **105**, 011119.
- 17 S. Aya, A. Zep, K. Aihara, K. Ema, D. Pocięcha, E. Gorecka, F. Araoka, K. Ishikawa and H. Takezoe, *Opt. Mater. Express*, 2014, **4**, 662.
- 18 H. J. Coles and M. N. Pivnenko, *Nature*, 2005, **436**, 997–1000.
- 19 I. Dierking, W. Blenkhorn, E. Credland, W. Drake, R. Kociuruba, B. Kayser and T. Michael, *Soft Matter*, 2012, **8**, 4355.
- 20 I. Dierking, *Polym. Chem.*, 2010, **1**, 1153.
- 21 W. He, G. Pan, Z. Yang, D. Zhao, G. Niu, W. Huang, X. Yuan, J. Guo, H. Cao and H. Yang, *Adv. Mater.*, 2009, **21**, 2050–2053.
- 22 N. Kasch, I. Dierking and M. Turner, *Soft Matter*, 2013, **9**, 4789.
- 23 H. Kikuchi, M. Yokota, Y. Hisakado, H. Yang and T. Kajiyama, *Nat. Mater.*, 2002, **1**, 64–8.
- 24 M. Ravnik, G. P. Alexander, J. M. Yeomans and S. Žumer, *Proc. Natl. Acad. Sci. U. S. A.*, 2011, **108**, 5188–92.
- 25 W. Cao, A. Muñoz, P. Palffy-Muhoray and B. Taheri, *Nat. Mater.*, 2002, **1**, 111–3.
- 26 E. Kemiklioglu, J.-Y. Hwang and L.-C. Chien, *Phys. Rev. E*, 2014, **89**, 042502.
- 27 M. S. Kim, Y. J. Lim, S. Yoon, S.-W. Kang, S. H. Lee, M. Kim and S.-T. Wu, *J. Phys. D: Appl. Phys.*, 2010, **43**, 145502.
- 28 M. S. Kim, Y. J. Lim, S. Yoon, M.-K. Kim, P. Kumar, S.-W. Kang, W.-S. Kang, G.-D. Lee and S. H. Lee, *Liq. Cryst.*, 2011, **38**, 371–376.
- 29 H. Lee, H.-J. Park, O.-J. Kwon, S. J. Yun, J. H. Park, S. Hong and S.-T. Shin, *SID Symp. Dig. Tech. Pap.*, 2011, **42**, 121–124.
- 30 S.-Y. Lu and L.-C. Chien, *Opt. Lett.*, 2010, **35**, 562–4.
- 31 O. Henrich, K. Stratford, M. E. Cates and D. Marenduzzo, *Phys. Rev. Lett.*, 2011, **106**, 107801.
- 32 M. S. Kim and L.-C. Chien, *Tracing three-dimensional topological defects in amorphous blue phase and inducing chirality by polymer molding*, Manuscript submitted.

- 33 M.-K. Kim, M. S. Kim, B. G. Kang, G. H. Yang, A. Mukherjee, S.-W. Kang, H. Lee, S.-T. Shin and S. H. Lee, *Mol. Cryst. Liq. Cryst.*, 2011, **543**, 194/[960]–199/[965].
- 34 Y. Hisakado, H. Kikuchi, T. Nagamura and T. Kajiyama, *Adv. Mater.*, 2005, **17**, 96–98.
- 35 L. Rao, J. Yan, S.-T. Wu, S. Yamamoto and Y. Haseba, *Appl. Phys. Lett.*, 2011, **98**, 081109.
- 36 J. Yan, Z. Luo, S.-T. Wu, J.-W. Shiu, Y.-C. Lai, K.-L. Cheng, S.-H. Liu, P.-J. Hsieh and Y.-C. Tsai, *Appl. Phys. Lett.*, 2013, **102**, 011113.
- 37 S.-W. Choi, S.-I. Yamamoto, T. Iwata and H. Kikuchi, *J. Phys. D: Appl. Phys.*, 2009, **42**, 112002.
- 38 N. Kim, D.-Y. Kim, M. Park, Y.-J. Choi, S. Kim, S. H. Lee and K.-U. Jeong, *Soft Matter*, 2015, **11**, 3772–9.
- 39 Y.-C. Yang, R. Bao, K. Li and D.-K. Yang, *SID Symp. Dig. Tech. Pap.*, 2009, **40**, 586.
- 40 L. Wang, W. He, X. Xiao, F. Meng, Y. Zhang, P. Yang, L. Wang, J. Xiao, H. Yang and Y. Lu, *Small*, 2012, **8**, 2189–93.
- 41 P.-J. Hsieh and H.-M. P. Chen, *Liq. Cryst.*, 2015, **42**, 216–221.
- 42 Y. Liu, S. Xu, D. Xu, J. Yan, Y. Gao and S.-T. Wu, *Liq. Cryst.*, 2014, **41**, 1339–1344.
- 43 L. Wang, W. He, X. Xiao, M. Wang, M. Wang, P. Yang, Z. Zhou, H. Yang, H. Yu and Y. Lu, *J. Mater. Chem.*, 2012, **22**, 19629.
- 44 P. Nayek, H. Jeong, S.-W. Kang, S. H. Lee, H.-S. Park, H. J. Lee, H. S. Kim and G.-D. Lee, *J. Soc. Inf. Disp.*, 2012, **20**, 318.
- 45 H. Iwamochi and A. Yoshizawa, *Appl. Phys. Express*, 2008, **1**, 111801.
- 46 S. Taushanoff, K. Van Le, J. Williams, R. J. Twieg, B. K. Sadashiva, H. Takezoe and A. Jákli, *J. Mater. Chem.*, 2010, **20**, 5893.
- 47 M. Sato and A. Yoshizawa, *Adv. Mater.*, 2007, **19**, 4145–4148.
- 48 P. J. Collings, *Phys. Rev. A*, 1984, **30**, 1990–1993.
- 49 J. Kerr, *Philos. Mag.*, 1875, **50**, 337–348.
- 50 J. W. Doane, A. Golemme, J. L. West, J. B. Whitehead and B.-G. Wu, *Mol. Cryst. Liq. Cryst. Inc. Nonlinear Opt.*, 1988, **165**, 511–532.
- 51 E. P. Koistinen and P. H. Keyes, *Phys. Rev. Lett.*, 1995, **74**, 4460–4463.

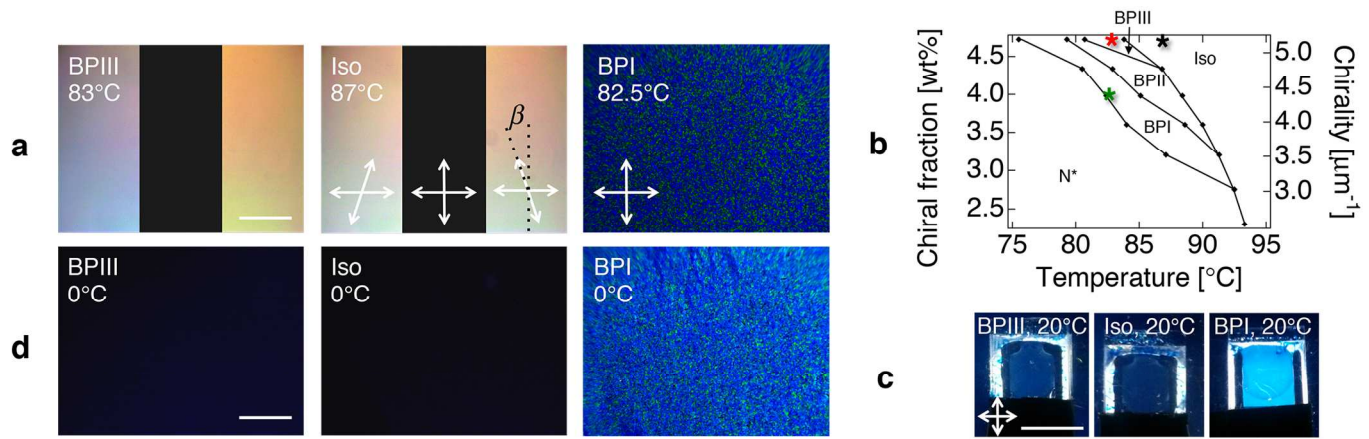


Fig. 1. (a) Photomicrographs of BPIII at 83 °C, isotropic phase at 87 °C and BPI at 82.5 °C before photo-polymerization. (b) Phase diagram of polymer and liquid crystal composite. Red, black and green stars correspond to BPIII, isotropic phase and BPI in (a), respectively. (c) Stabilized cells viewed between crossed polarizers on a white backlight. (d) Photomicrographs at 0 °C after photo-polymerization. White arrows indicate the optic axes of polarizers with a deviation angle  $\beta = \pm 3^\circ$ . Scale bars are (a, d) 500  $\mu\text{m}$  and (c) 1 cm.

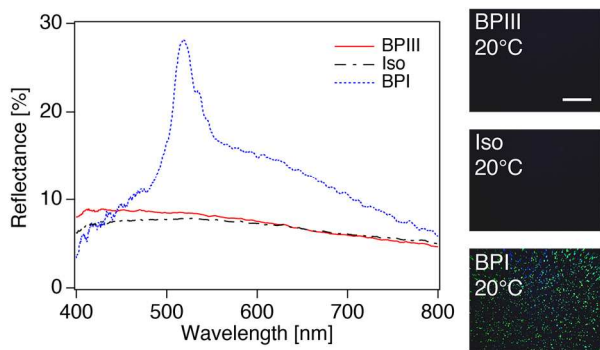


Fig. 2. Reflection spectra of stabilized phases and polarizing optical micrographs in reflection mode. Scale bar is 500  $\mu\text{m}$ .

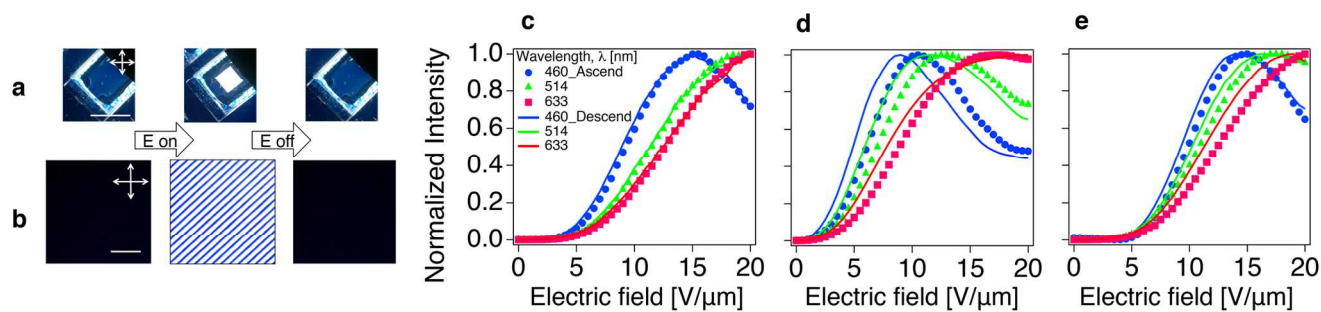


Fig. 3. (a) Switching of the stabilized BPIII cell by the applied electric field  $E = 18.5 \text{ V}/\mu\text{m}$  between crossed polarizers on a white backlight and (b) corresponding polarizing optical micrographs. White arrows indicate the optic axes of polarizers. Scale bars are (a) 1 cm and (b)  $50 \mu\text{m}$ . (c-e) Transmittance versus applied electric field curves of the stabilized (c) BPIII, (d) isotropic phase and (e) BPI. Red, green and blue represent specified wavelengths of 633, 514 and 460 nm, respectively.<sup>‡</sup>

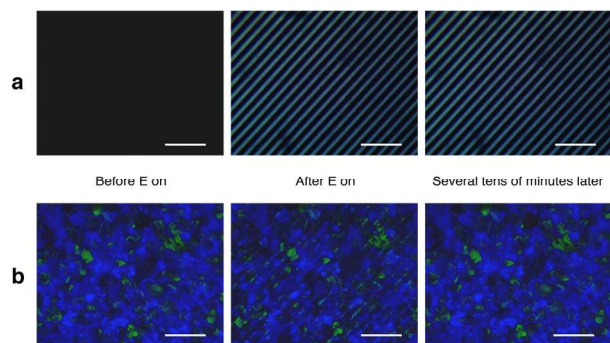


Fig. 4. Polarizing optical micrographs of (a) isotropic phase and (b) BPI before, after and several minutes after turning off the applied electric fields  $E = 11$  and  $17 \text{ V}/\mu\text{m}$ , respectively. Scale bars are  $50 \mu\text{m}$ .

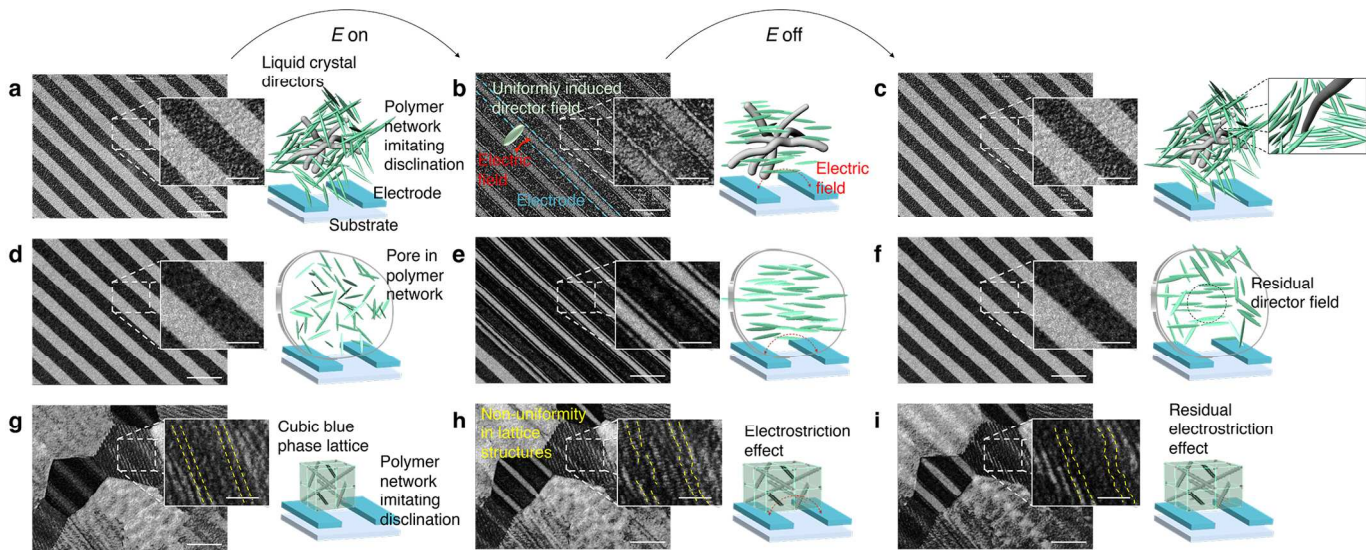


Fig. 5. Confocal laser scanning micrographs before and after applying the electric field to the stabilized (a-c) BPIII, (d-f) isotropic phase, and (g-i) BPI. Insets are zoomed in from the region of white broken rectangles. Right side columns are schematic illustrations of each state with liquid crystal directors (green) and polymer (gray) on a substrate (light blue) with patterned electrodes (greenish blue). Scale bars are 15  $\mu\text{m}$  and 5  $\mu\text{m}$  in insets. Yellow broken lines in insets of (g-i) indicate topological lattice patterns in a grain. Inset of schematic illustration in (c) indicates polymer and local director field. The singularity is not able to escape into third-dimension and pertains the disclinations in BPs.

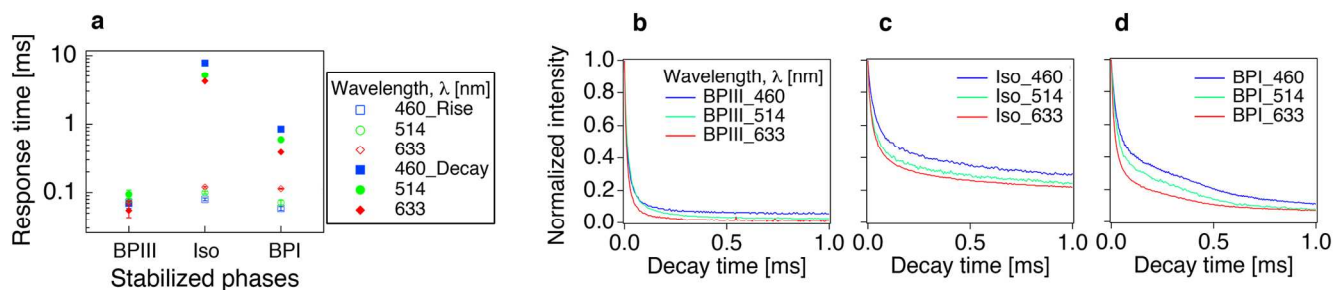


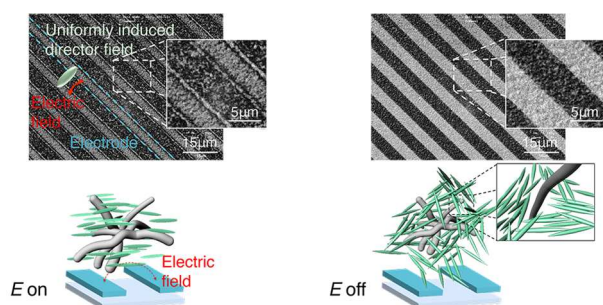
Fig. 6. (a) Electro-optic response time of the stabilized BPIII, isotropic phase and BPI. Empty and filled markers indicate rise and decay time, respectively. Error bars were acquired from the experimental standard deviation of 10 repeated measurements. (b-d) The transmittance with respect to decay time of three stabilized phases with red, green and blue curves representing specified wavelengths of 633, 514 and 460 nm, respectively.

## Topology-mediated electro-optical behaviour of wide-temperature liquid crystalline amorphous blue phase

Min Su Kim\* and Liang-Chy Chien

Liquid Crystal Institute & Chemical Physics Interdisciplinary Program, Kent State University, Kent, OH 44242, USA.

\*E-mail: mkim12@kent.edu



The polymer-stabilized amorphous blue phase manifests tens of microsecond response time, a consistent achromatic dark state and intrinsically electro-optical hysteresis-free.